High-spatial-resolution strain sensor based on distance compensation and image wavelet denoising method in OFDR

Pengfei Li, Cailing Fu, Bin Du, Jun He, Huajian Zhong, Chao Du, Lei Wang, Yiping Wang, *Member, IEEE*

***Abstract*—A high-spatial-resolution strain sensor in OFDR was experimentally demonstrated by use of combining distance compensation (DC) and image wavelet denoising (IWD) method. Compared with using one method alone, the measured distribution strain could be varied from 200 to 2000 με at a spatial resolution of 2.56 mm. Moreover, four times enhancement of the accuracy for the strain senor was achieved without hardware modification. This method is a significant step toward a high performance OFDR system, especially for evaluating the rapid change of object's structural condition.**

***Index Terms*—Optical frequency domain reflectometry, distributer strain sensor, distance compensation, image wavelet denoising**

I. INTRODUCTION

An optical frequency domain reflectometry (OFDR) based on distributed strain sensing system has been widely used in various nondestructive diagnoses fields such as structural health monitoring [1]-[3], small mechanical structures measuring [4] and 3-dimensional (3D) shape sensing [5], [6]. Compared with Brillouin optical time domain analysis (BOTDA) [7] and phase optical time domain reflectometer (φ-OTDR) [8], OFDR could achieve a higher spatial resolution and higher sensitivity. However, the commercial and currently reported OFDR system (OBR 4600, LUNA) could only perform with a centimeter-range spatial resolution, which was limited by the nonlinear frequency modulation of tunable laser source (TLS), correlation noise, detector intensity noise and ambient vibration noise [9]. To improve the performance of the strain sensor based on OFDR, various data processing methods were proposed and demonstrated, such as suppressing the cross-correlation [10] fake peaks and multi-peaks using the method based on the local similar characteristics of an Rayleigh scattering (RS) fingerprint spectrum [11], avoiding the interaction between spatial and spectral resolution using the method based on Morlet wavelet transform [12] and decreasing common-mode residual nonlinear phase and favor phase unwrapping using the method based on differential relative phase [13], reducing the deterioration induced by position segment mismatch using the method based on distance compensation, i.e., combining spatial calibration and spectrum registration [14]. According to Ref. [15], the distance compensation method could only be used in the case of a small disturbance of noise situation. Moreover, the obtained OFDR strain data are limited to 1-dimensional (1D) arrays by the afore-mentioned methods [11]-[14], resulting in abandoning the multi-dimensional domain of the useful signal. As we know, when the strain was applied to fiber, the phenomenon of position deviation would be occurred, resulting in the deterioration of the amplitude for the cross-correlation between the reference and measurement signal, which limited the ability of 2D processing algorithm to achieve a larger strain measurement with a higher spatial resolution. 2-dimensional (2D) image denoising including non-mean [15] and bilateral filter method [16] has been used in BOTDA and φ-OTDR [17], [18]. However, few reports have been reported in OFDR by use of the 2D image denoising method to improve the performance of distributed strain sensor in OFDR. In addition, the position deviation and system noise could not be completely eliminated only by distance compensation or image denoising in OFDR system.

In this letter, a high-spatial-resolution strain sensor was proposed and demonstrated in OFDR by use of combining the

Manuscript received XXXX, 2021; revised XXXX, 2021; accepted XXXX, 2021. Date of publication XXXX, 2021; date of current version XXXX, 2021. This work was supported in part by National Natural Science Foundation of China (NSFC) (61635007, 61905155); Natural Science Foundation of Guangdong Province (2019A050510047, 2019B1515120042); Science and Technology Innovation Commission of Shenzhen Municipality (JCYJ 20200109114201731, JCYJ20200109114020865) and The Shenzhen Key Laboratory of Photonic Devices and Sensing Systems for Internet of Things.

P. Li, C. Fu, B. Du, J. He, H. Zhong, C. Du, L. Wang, Y. Wang are with the Key Laboratory of Optoelectronic Devices and Systems of Ministry of Education and Guangdong Province, College of Physics and Optoelectronic Engineering, Shenzhen University, Shenzhen 518060, China and are also with Shenzhen Key Laboratory of Photonic Devices and Sensing Systems for Internet of Things, Guangdong and Hong Kong Joint Research Centre for Optical Fibre Sensors, Shenzhen University, Shenzhen 518060, China (e-mail: lipengfei2022@163.com; fucailing@szu.edu.cn; dubean@126.com; hejun07@szu.edu.cn; 1748996356@qq.com; 770839949@qq.com; ypwang@szu.edu.cn)

L. Wang is with Shenzhen Key Laboratory of Polymer Science and Technology, College of Materials Science and Engineering, Shenzhen University, Xueyuan Avenue 1066, Nanshan, Shenzhen, 518055, China (e-mail: wl@szu.edu.cn)

(*Corresponding author e-mail: fucailing@szu.edu.cn)

distance compensation (DC) and image wavelet denoising (IWD) method, i.e., DC+IWD method. The effect of different similarity calculation methods, i.e., traditional method and Euclidean-, Cosine-, Pearson-based similarity DC method, on the cross-correlation shift and amplitude were investigated along the distributed strain sensor. Moreover, the influence of the traditional method, DC method, IWD method, and DC+IWD method on the demodulation strain profile and strain variation was also discussed to accurately remove the noise from the acquired OFDR data for achieving a high-spatial-resolution distributed strain sensing.

II. Experimental Setup and Methods

An experimental setup based on OFDR was built for distributed strain sensing, as illustrated in Fig. 1. Light from a TLS (81940A, Keysight) is divided into two parts, i.e., the auxiliary interferometer (AI) and the main interferometer (MI), by a 10:90 optical coupler (OC), i.e., OC_1. where the AI is mandatory for the system. The AI, i.e., a Michelson interferometer, consists of two faraday rotating mirrors (FRMs, Thorlabs), i.e., FRM_1 and FRM_2, which are used to reduce the polarization fading, and a delay fiber with a length of 70 m, i.e., L_2 = 70 m. The clock signal generated by the AI is used to trigger a data acquisition card (DAQ, PCI 6115, NI) through the balanced photodetector (BPD, 480C, Thorlabs), i.e., BPD_1, which samples the interference signal at equidistant instantaneous optical frequency points to suppress the nonlinearity in the frequency sweeping of the TLS [19], where the acquisition rate of the employed DAQ is 3.5 MS/s. The MI is consisted of a Mach-Zehnder interferometer formed by two 50:50 OCs, i.e., OC_2 and OC_3. One arm is connected to a distributed sensor, i.e., a section of standard single mode fiber (SMF), through a circulator (CIR), i.e., CIR_2, and the other is used as the reference light, where the length of the tested SMF is 25 m, i.e., L_1 = 25 m. A polarization controller (PC) is employed to adjust the polarization state within the main interferometer. The acquired signal, i.e., Rayleigh scattering (RS), is split into p/s polarization light through two polarization beam splitters (PBSs), i.e., PBS_1 and PBS_2, and then are converted into electrical signals by two BPDs, i.e., BPD_2 and BPD_3, and then collected by DAQ for the data processing.

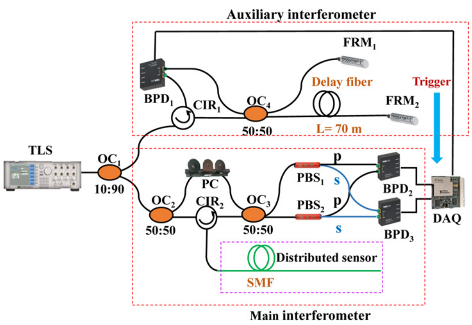

Fig. 1 Experimental setup based on OFDR for distributed strain sensing. TLS: tunable laser source; OC: optical coupler; CIR: circulator; FRM: faraday rotating mirror; BPD: balanced photo-detector; PC: polarization controller; SMF: single mode fiber; PBS: polarization beam splitter; DAQ: data acquisition card. The length of the tested and delay fiber is 25 and 70 m, i.e., L_1 = 25 m, L_2 = 70 m, respectively.

As we know, the backward RS in SMF is induced by the inhomogeneities refractive-index-distributed in the core of optical fiber, and the RS is stable once the SMF is fabricated. The RS will change accordingly when different strains are applied to the SMF. Moreover, the OFDR is a distributed optical fiber sensing technology based on obtained backward RS. Thus, the reference signal in the OFDR strain system is defined as the beat frequency signal, i.e., the original backward RS, acquired by the DAQ, as illustrated in Fig. 1, when there is no strain, while the measurement signal is the measured backward RS when the strain is applied. According to Ref. [9], [20], the position-deviation induced by the change of optical path due to the thermal-/elastic-optic effect will be accumulated along the fiber when the strain is applied, resulting in the deterioration of the cross-correlation spectra in the frequency domain, especially in the stretched-strain section.

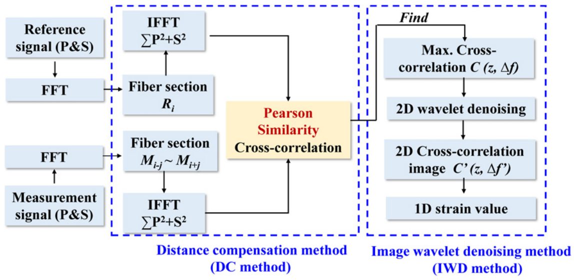

Fig. 2 Flow chart of the strain data processing using the method based on combining distance compensation and image wavelet denoising (DC+IWD). R_i (i = 1, 2, 3…) represents the i-th represents reference signal in time-domain; M_{i-j}, M_{i+j} ($i-j \geq 1$, j = 10) represents the (i-j)-th, (i+j)-th measurement signal in time-domain, respectively. FFT: Fast Fourier Transformation (FFT); IFFT: inverse FFT; 1D: 1-dimensional; 2D: 2-dimensional.

To maintain the cross-correlation amplitude of the RS spectra, i.e., obtain a higher spatial resolution and larger strain range, a method based on combining distance compensation and image wavelet denoising (DC+IWD) was proposed, as illustrated in Fig. 2. The detailed flow chart of strain data processing is divided into two steps, i.e., DC and IWD method, labeled by the blue dotted box. As shown in Fig. 2, the strain distributed sensor, i.e., standard SMF in Fig. 1, is evenly divided into several sections with the same length, i.e., R_i (i = 1, 2, 3…) and M_{i-j} - M_{i+j} ($i-j \geq 1$, j = 10) for the reference and measurement signal in time domain, respectively, by using Fast Fourier Transformation (FFT), where the p/s polarization light of each section in time domain could be transformed into frequency domain via inverse FFT (IFFT). And then the cross-correlation operation with different similarity calculation methods was carried out between the reference and measurement signal after vector sum for p/s polarization to find out the specific position of the fiber corresponding to the cross-correlation shift at the maximum cross-correlation amplitude to reduce the position deviation. In this step, the cross-correlation matrix data can be obtained, i.e., C $(z, \Delta f)$, where z and Δf is the distance of the fiber sensor and shift of the cross-correlation, respectively. Then another 2D cross-correlation image matrix data, i.e., C' $(z, \Delta f')$, could be obtained through the graying process and 2D wavelet denoising algorithm including the 2D wavelet transform, shrinkage and inverse wavelet transform, where the $\Delta f'$ is the optimized cross-correlation shift.

Finally, the value of applied 1D strain could be calculated using the relationship between the cross-correlation shift, i.e., $\Delta f'$, and strain, i.e., ε, which could be established by the equation

$$\varepsilon = k \times \Delta f' \tag{1}$$

where k is the strain sensitivity coefficient of the SMF, and k = 6.67 με/GHz.

In addition, the two-point spatial resolution, i.e., Δz, in time domain could be given by

$$\Delta z = c / 2n\Delta F \tag{2}$$

where c is the light velocity in vacuum, n is the refractive index of the medium, ΔF is the range of the sweep frequency of the TLS. In the experiment, the TLS is swept from 1545 to 1555 nm with a speed rate of 40 nm/s, indicating that the ΔF = 1250 GHz. Therefore, Δz could be calculated to 0.08 mm. Then the sensing spatial resolution could be given by

$$z = N \times \Delta z \tag{3}$$

where N is the number of data point, and N = 32. This indicated that the sensing spatial resolution is 2.56 mm, i.e., z = 2.56 mm, of the strain sensor based on OFDR.

III. Experimental Results and Discussions

To verify the proposed method, i.e., DC+IWD method, the experimental setup for strain sensing was built, as illustrated in Fig. 3(a), where the translation stage was used to apply the strain along the axis of the SMF. As shown in Fig. 3(a), the distributed strain sensor could be divided into the zero-strain, i.e., section-A, -C, and -E, and the stretched-strain section, i.e., section-B and -D, where the length of the section-B, -C and -D are 0.50, 0.12 and 0.50 m, respectively. It is well known that the amplitude of the cross-correlation characterizes the similarity between the reference and measurement signal in frequency domain using DC method in Fig. 2. The larger amplitude of the cross-correlation is, the higher the similarity is, and the smaller position deviation is [19]. As shown in Fig. 3(b), the cross-correlation shift with different similarity calculation methods, i.e., the traditional method and the Euclidean-, Cosine-, Pearson-based similarity DC method, respectively, was calculated to be -17.83, 0, 57.3, 0 GHz at a distance of 20.202 m in the section-C, i.e., zero-strain section, corresponding to the maximum amplitude r_1 = 0.3557, r_2 = 0.8755, r_3 = 0.3261, r_4 = 0.8755, respectively, indicating that the Euclidean- and Pearson-based similarity DC method have a larger amplitude at the zero-strain condition, where the cross-correlation shift is equal to zero. Moreover, the amplitude of the cross-correlation at random position in the zero-strain and stretched-strain, i.e., section-A to section-E, are calculated by use of the afore-mentioned methods. The calculated amplitudes labeled by the black, purple, blue and red symbol, respectively, are illustrated in Fig. 3(c), where the amplitude is between 0 and 1. Here the traditional method was defined as the cross-correlation between the reference and measurement signal without extra processing. As shown in Fig. 3(c), Pearson-based similarity DC method has a maximum amplitude from section-A to section-E. Therefore, the Pearson-based similarity DC method is better to achieve a maximum cross-correlation to improve the image wavelet denoising effect.

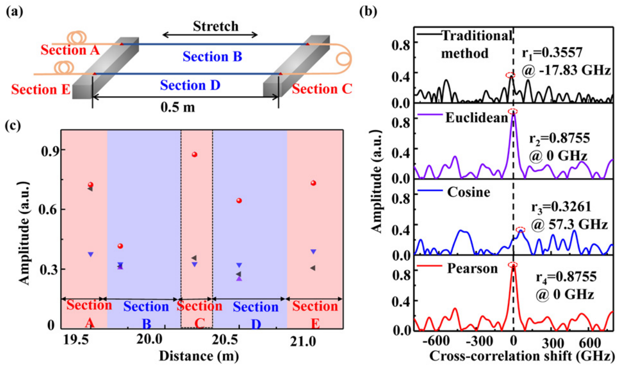

Fig. 3 (a) Schematic diagram of the strain sensing experimental setup in which the employed fiber, i.e., SMF, is divided into the zero-strain section (section-A, -C, and –E) and the stretched-strain section (section-B and -D); (b) The cross-correlation shift at a position of 20.202 m in the zero-strain, i.e., section-C, using the traditional method and the Euclidean-, Cosine-, Pearson-based similarity DC method, respectively; (c) The calculated cross-correlation amplitude using the traditional method (◀) and the Euclidean- (▲), Cosine- (▼), Pearson-based (●) similarity DC method, respectively.

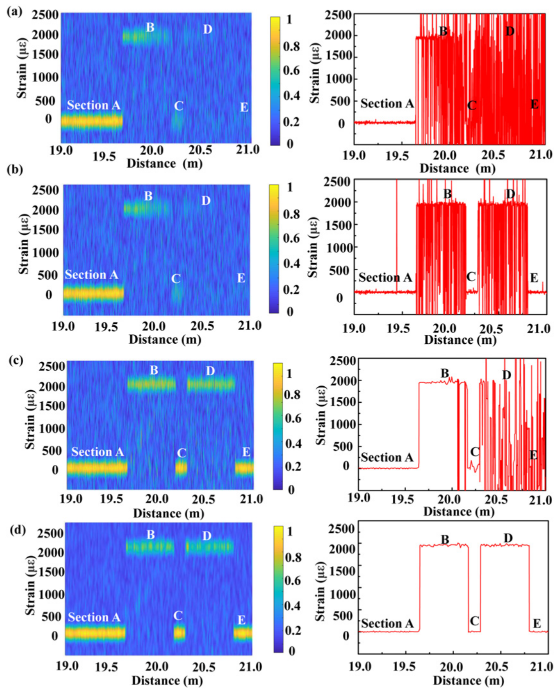

Fig. 4 Obtained demodulation strain profiles processed by the (a) traditional method, (b) DC method, (c) IWD method, and (d) DC+IWD method, while the applied strain is 2000 με and a spatial resolution of 2.56 mm is supposed. The wavelet function is sym7, the level of decomposition is set to 3, and threshold value is 0.0664.

According to the flow chart in Fig. 2, the maximum cross-correlation matrix data, i.e., $C(z, \Delta f)$, could be obtained by traversing the whole distributed sensor fiber using the Pearson-based similarity DC method. Then the matrix $C(z, \Delta f)$ was converted into $C'(z, \Delta f')$ using the gray processing and 2D wavelet denoising method. In the experiment, the gray processing was used to transform the obtained maximum cross-correlation matrix data, i.e., $C\ (z, \Delta f)$, into a gray image. The detailed process was to normalize the matrix, i.e., $C\ (z, \Delta f)$, between 0-255, and then convert the type of the afore-obtained data from double to unit8. During the process using the 2D wavelet denoising method, the wavelet function, decomposition level, and threshold value are vital parameters. In the experiment, the sym7 is employed as the wavelet function to obtain a better denoising capability, where 7 is the order of wavelet function. Moreover, the decomposition level is set to 3 to decrease the distortion of cross-correlation spectrum. As for the noise standard deviation is 0.0197, i.e., σ = 0.0197, the threshold value is set to approximately 3.4 times of standard deviation, i.e., 0.0664. Then the demodulation strain profile processed by the traditional method, DC method, IWD method and DC+IWD method are illustrated in Figs. 4(a), 4(b), 4(c) and 4(d), respectively, when the applied strain is 2000 με and the spatial resolution is 2.56 mm.

As shown in Fig. 4(a), only section-A could be clearly observed, while section-B, -C, -D and -E were submerged in noise using the traditional method, and the noise signal were accumulated along the fiber. In Fig. 4(b), the zero-strain, i.e., section-A, -C, and -E were effectively improved, while the stretched-strain section, i.e., section-B and -D, were also submerged in noise using the DC method. Then section-A, -B and -C could be demodulated by using the IWD method, while the noise signal in the section-D and -E could not be eliminated, as illustrated in Fig.4 (c). Compared with Figs. 4(a), 4(b) and 4(c), the zero-strain and stretched-strain section, i.e., section-A to -E, could be successfully demodulated by the DC+IWD method, as illustrated in Fig. 4(d), indicating that the strain signal could be accurately recovered from the noise to improve the spatial resolution of the OFDR system by combing the DC method and IWD method, i.e., DC+IWD method.

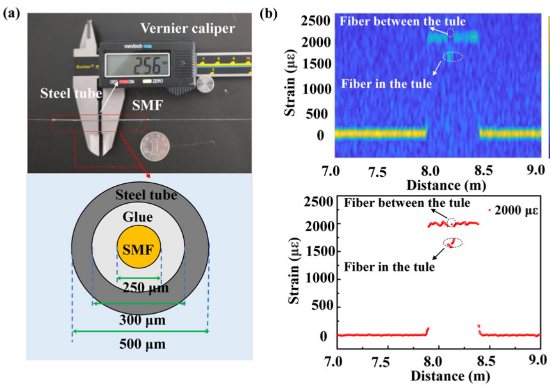

Fig. 5 (a) Schematic experimental setup to verify the spatial resolution; (b) Obtained demodulation strain profile when the strain of 2000 με was applied.

To verify the afore-obtained spatial resolution, i.e., 2.56 mm, two ends of the sensing fiber, i.e., single mode fiber (SMF), are placed into two steel tubes with an inner, outer diameter and length of 0.3, 0.5 and 40 mm, respectively, using the glue to encapsulate and fix the SMF, where the distance between two steel tubes is 2.56 mm, as illustrated in Fig. 5(a). The demodulation strain profile was illustrated in Fig. 5(b) using the DC+IWD method when the strain of 2000 με was applied. As shown in Fig. 5(b), the fiber between and in the steel tube could be clearly observed, indicating that the spatial resolution agreed well with the theoretical value, i.e., 2.56 mm.

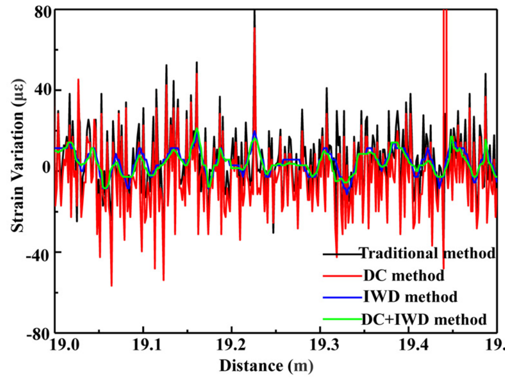

Fig. 6 The strain variation in the section-A, i.e., zero-strain, which are derived from the data processed by the traditional method, DC method, IWD method, and DC+IWD method, labeling by the black, red, blue, and green curve, respectively.

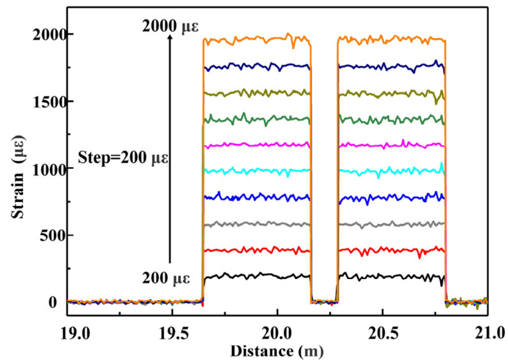

Fig. 7 Calculated demodulation strain profiles using the DC+IWD method, while the strain increased from 200 to 2000 με with a step of 200 με and the spatial resolution was 2.56 mm.

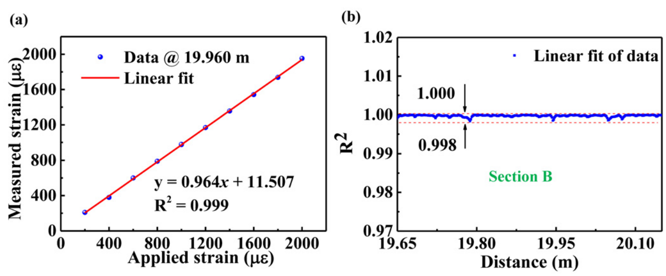

Fig.8 Measured strain as a function of the applied strain at (a) the distance of 19.96 m and (b) section B when the strain increased from 200 to 2000 με

Moreover, the influence of different methods on the demodulated strain variation in the section-A, i.e., zero-strain section, was investigated. The traditional method and DC method are 1D processing, while IWD and DC+IWD method are 2D processing. As shown in Fig. 6, the strain variation, i.e., accuracy of the demodulated strain with 1D processing, i.e., traditional method and DC method, and 2D processing, i.e., IWD and DC+IWD method, is ± 80 and ± 20 με, respectively, labeled by the black, red, blue, and green curve, respectively.

This indicated that the accuracy of the distributed strain sensor based on OFDR could be increase to four times using the DC+IWD method. To verify the generality of the proposed DC+IWD method, the demodulation strain profiles were calculated while the strain was increased from 200 to 2000 με with a step of 200 με. As shown in Fig. 7, the zero-strain and stretched-strain section, i.e., section-A to section–E, could be clearly recovered by the DC+IWD method. As shown in Fig. 8(a), the measured strain linearly changed with applied strain with a slope and R^2 of 0.964 and 0.999, respectively, at the distance of 19.96 m in Fig.7, when the strain increased from 200 to 2000 με. Moreover, the R^2, i.e., 0.998 to 1.000, in section B was also calculated, as illustrated in Fig. 8(b), indicating that the measured strain is almost equal to the applied strain. The result of a 2.56 mm sensing spatial resolution is better than the LUNA OBR4600 [21] and LUNA ODISI-B [22] which is the leading level of OFDR.

IV. Conclusion

In conclusion, a method combining DC and IWD method, i.e., DC+IWD method, was proposed and demonstrated to obtain a high-spatial-resolution strain sensor based on OFDR. Compared with the traditional method, and the Euclidean-, Cosine-based similarity DC method, the Pearson-based similarity DC method is optimal to achieve a maximum cross-correlation to improve the image denoising effect. Moreover, the zero-strain and stretched-strain section could be successfully demodulated for the distributed strain sensor at a spatial resolution of 2.56 mm using the DC+IWD method, when the applied strain is from 200 to 2000 με. Furthermore, the accuracy of the demodulated strain was enhanced from ± 80 to ± 20 με by the DC+IWD method. Hence, this method could be used to achieve a larger distributed strain measurable range at a high spatial resolution for OFDR system without the hardware modification.

References

[1]. S. Rizzolo, J. Perisse, A. Boukenter, Y. Ouerdane, E. Marin, J. R. Mace, M. Cannas, and S. Girard, "Real time monitoring of water level and temperature in storage fuel pools through optical fibre sensors," *Sci. Rep.*, vol. 7, no. 1, pp: 8766, Aug. 2017.

[2]. P. Zhu, X. Xie, X. Sun, and M. A. Soto, "Distributed modular temperature-strain sensor based on optical fiber embedded in laminated composites," *Compos. B. Eng.*, vol. 168, pp: 267-273, Dec. 2019.

[3]. Y. Liu, L. Chen, W. Liu, X. Liang, and W. Wan, "Resolution-enhanced imaging through scattering media by high-order correlation," *Appl. Opt.*, vol. 58, no. 9, pp: 2350-2357, Mar. 2019.

[4]. L. Peng, J. Li, R. A. McLaughlin, H. Ebendorff-Heidepriem, and S. C. Warren-Smith, "Distributed optical fiber sensing of micron-scale particles," *Sens Actuator A-Phys.*, vol. 303, pp: 111762, Mar. 2020.

[5]. G. Sun, H. Li, M. Dong, X. Lou, and L. Zhu, "Optical fiber shape sensing of polyimide skin for a flexible morphing wing," *Appl. Opt.*, vol. 56, no. 33, pp: 9325-9332, Nov. 2017.

[6]. M. Amanzadeh, S. M. Aminossadati, M. S. Kizil, and A. D. Rakić, "Recent developments in fibre optic shape sensing," *Measurement*, vol. 128, pp: 119-137, Nov. 2018.

[7]. P. Lu, N. Lalam, M. Badar, B. Liu, B. T. Chorpening, M. P. Buric, and P. R. Ohodnicki, "Distributed optical fiber sensing: Review and perspective," *Appl. Phys. Rev.*, vol. 6, no. 4, pp: 041302, Dec. 2019.

[8]. Z. Zhang, X. Fan, and Z. He, "Long-range and wide-band vibration sensing by using phase-sensitive OFDR to interrogate a weak reflector array," *Opt. Express*, vol. 28, no. 12, pp: 18387-18396, Jun. 2020.

[9]. R. Chen, Z. Peng, M. Wang, A. Yan, S. Li, S. Huang, M. J. Li, and K. P. Chen, "Spatially resolved fibre cavity ring down spectroscopy," *Sci. Rep.*, vol. 10, no. 1, pp: 20167, Nov. 2020.

[10]. M. Froggatt, J. Moore, "High-spatial-resolution distributed strain measurement in optical fiber with Rayleigh scatter," *Appl. Opt.*, vol. 37, no. 10, pp: 1735-1740, Apr. 1998.

[11]. K. Feng, J. Cui, D. Jiang, H. Dang, Y. Jin, X. Sun, Y. Niu, and J. Tan, "Improvement of the strain measurable range of an OFDR based on local similar characteristics of a Rayleigh scattering spectrum," *Opt. Lett.*, vol. 43, no. 14, pp: 3293-3296, Jul. 2018.

[12]. K. Feng, J. Cui, H. Dang, D. Jiang, Y. Jin, X. Sun, and X. Zhang, "A OFDR Signal Processing Method Based on Wavelet Transform for Improving Its Sensing Performance," *IEEE Photon. Technol. Lett.*, vol. 31, no. 13, pp: 1108-1111, Jul. 2019.

[13]. C. Wang, K. Liu, Z. Ding, J. Jiang, Z. Chen, Y. Feng, Y. Zheng, Q. Liu, and T. Liu, "High Sensitivity Distributed Static Strain Sensing Based on Differential Relative Phase in Optical Frequency Domain Reflectometry," *J. Lightwave Technol.*, vol. 38, no. 20, pp: 5825-5836, Oct. 2020.

[14]. S. Zhao, J. Cui, L. Suo, Z. Wu, D.-P. Zhou, and J. Tan, "Performance Investigation of OFDR Sensing System With a Wide Strain Measurement Range," *J. Lightwave Technol.*, vol. 37, no. 15, pp: 3721-3727, Aug. 2019.

[15]. H. Wu, L. Wang, Z. Zhao, N. Guo, C. Shu, and C. Lu, "Brillouin optical time domain analyzer sensors assisted by advanced image denoising techniques," *Opt. Express*, vol. 26, no. 5, pp: 5126-5139, Mar. 2018.

[16]. H. He, L. Shao, H. Li, W. Pan, B. Luo, X. Zou, and L. Yan, "SNR Enhancement in Phase-Sensitive OTDR with Adaptive 2-D Bilateral Filtering Algorithm," *IEEE Photon. J.*, vol. 9, no. 3, pp: 1-10, Jun. 2017.

[17]. M. A. Soto, J. A. Ramirez, and L. Thevenaz, "Optimizing Image Denoising for Long-Range Brillouin Distributed Fiber Sensing," *J. Lightwave Technol.*, vol. 36, no. 4, pp: 1168-1177, Feb. 2018.

[18]. X. Qian, X. Jia, Z. Wang, B. Zhang, N. Xue, W. Sun, Q. He, and H. Wu, "Noise level estimation of BOTDA for optimal non-local means denoising," *Appl. Opt.*, vol. 56, no. 16, pp: 4727-4734, Jun. 2017.

[19]. M. E. Froggatt, D. K. Gifford, S. Kreger, M. Wolfe, and B. J. Soller, "Characterization of Polarization-Maintaining Fiber Using High-Sensitivity Optical-Frequency-Domain Reflectometry," *J. Lightwave Technol.*, vol. 24, no. 11, pp. 4149-4154, Nov. 2006.

[20]. M. Luo, J. Liu, C. Tang, X. Wang, T. Lan, and B. Kan, "0.5 mm spatial resolution distributed fiber temperature and strain sensor with position-deviation compensation based on OFDR," *Opt. Express*, vol. 27, no. 24, pp: 35823-35829, Nov. 2019.

[21]. LUNA-Data-Sheet-OBR-4600-V2 [Online]. Available: https://lunainc.com/sites/default/files/assets/files/resource-library/LUNA-Data-Sheet-OBR-4600-V2.pdf.

[22]. ODB5_DataSheet [Online]. Available: https://lunainc.com/sites/default/files/assets/files/data-sheet/ODB5_DataSheet_Rev13_020217.pdf.

Pengfei Li was born in Henan, China, in 1991. She received the M.S. degree in school of physics and engineering from Henan university of science and technology in 2019. She is currently pursuing the Ph.D. degree in optical engineering at Shenzhen University.

Cailing Fu was born in Hubei, China, in 1989. She received the M.S. degree in optical engineering from Wuhan Institute of Technology, Wuhan, China, in 2015, and the Ph.D. degree in optical engineering in Shenzhen University in 2018. From 2018 to 2020, she was with information and communication engineering of Shenzhen University, as a post-doc Research Fellow. Since Sept., 2020, she has been in Shenzhen University, Shenzhen, China, as an Assistant Professor. Her current research interests focus on distributed optical fiber sensing technology. She has authored or coauthored have more than 30

journal and conference papers.

Bin Du was born in Henan China, in 1992. He received the B.S. degree in Flight Vehicle Propulsion Engineering in School of Astronautics from Beihang University, in 2016. His current research interests focus on fiber vibration and ultrasound sensor.

Jun He was born in Hubei, China, in 1985. He received the B.Eng. degree in electronic science and technology from Wuhan University, Wuhan, China, in 2006 and the Ph.D. degree in electrical engineering from the Institute of Semiconductors, Chinese Academy of Sciences, Beijing, China, in 2011. From 2011 to 2013, he was with Huawei Technologies, Shenzhen, China, as a Research Engineer. From 2013 to 2015, he was affiliated with Shenzhen University, Shenzhen, as a Postdoctoral Research Fellow. From 2015 to 2016, he was with The University of New South Wales, Sydney, Australia, as a Visiting Fellow. Since 2017, he has been with Shenzhen University as an Assistant Professor. His current research interests include optical fiber sensors, fiber Bragg gratings, and fiber lasers. He has authored or co-authored four patent applications and more than 80 journal and conference papers. He is a Member of the Optical Society of America.

Huajian Zhong was born in Jiangxi China, in 1998. He received his B.S. degree from Changchun University of Science and Technology in 2020. His current research interest is distributed optical sensing.

Chao Du was born in Shanxi China, in 1998. He received a B.S. degree from the School of Physics and Optoelectronic Engineering of Taiyuan University of Technology in 2020. He is currently pursuing the M.S. degree in optical engineering at Shenzhen University.

Lei Wang was born in Shandong, China, in 1977. He is currently the full professor in the college of materials science and engineering at Shenzhen University. His research includes functional fluorescent materials, thermoelectric materials, and ion exchange membranes.

Yiping Wang (SM'11) was born in Chongqing, China, in 1971. He received the B.Eng. degree in precision instrument engineering from Xi'an Institute of Technology, China, in 1995 and the M.S. degree and Ph.D. degree in optical engineering from Chongqing University, China, in 2000 and 2003, respectively. From 2003 to 2005, he was with Shanghai Jiao Tong University, China, as a Postdoctoral Fellow. From 2005 to 2007, he was with the Hong Kong Polytechnic University, as a Postdoctoral Fellow. From 2007 to 2009, he was with the Institute of Photonic Technology (IPHT), Jena, Germany, as a Humboldt Research Fellow. From 2009 to 2011, he was with the Optoelectronics Research Centre (ORC), University of Southampton, U.K., as a Marie Curie Fellow. Since 2012, he has been with Shenzhen University, Shenzhen, China, as a Distinguished Professor. His current research interests focus on optical fiber sensors, fiber gratings, and photonic crystal fibers. He has authored or coauthored 1 book, 21 patent applications, and more than 240 journal and conference papers. Prof. Wang is a Senior Member of IEEE, the Optical Society of America, and the Chinese Optical Society.